第 40 卷 第 3 期 焊 接 学 报 Vol. 40(3):128 − 132
2019 年 3 月 TRANSACTIONS OF THE CHINA WELDING INSTITUTION March 2019

转速对 6082-T6 铝合金搅拌摩擦焊焊接接头织构的影响

张亮亮[1], 王希靖[1,2], 魏学玲[1], 刘 骁[1], 柴廷玺[3]

(1. 兰州理工大学 省部共建有色金属先进加工与再利用国家重点实验室, 兰州 730050; 2. 兰州理工大学 材料科学与工程学院, 兰州 730050; 3. 兰州城市学院 培黎机械工程学院, 兰州 730070)

摘 要: 采用电子背散射衍射技术, 借助取向成像分析软件, 研究了搅拌头在不同转速下, 6082-T6 铝合金搅拌摩擦焊焊核区上表面晶粒形貌、晶界特征、织构组分的演化. 结果表明, 在搅拌针所引入的剪切应力作用下, 焊核区形成 (110)[001] 高斯织构和 (114)[22$\bar{1}$] 织构, 轴肩的顶锻压力使其沿着 TD 方向旋转一定角度, 形成 (112)[11$\bar{1}$] 铜织构, 随着搅拌头转速的提高, 晶粒沿着 TD 方向旋转角度增加, 进一步形成 (100)[011] 剪切织构和 (11$\bar{1}$)[112] 织构; 焊核区晶粒受到搅拌针的挤压而形成 [110] 丝织构, 搅拌头转速从 1 200 r/min 提高到 2 000 r/min 时, 挤压程度增加, 导致 [110] 丝织构组分显著增多.

关键词: 6082-T6 铝合金; 搅拌摩擦焊; 晶粒取向演化; 电子背散射衍射

中图分类号: TG 453.9 **文献标识码:** A **doi:** 10.12073/j.hjxb.2019400085

0 序 言

搅拌摩擦焊 (friction stir welding, FSW) 是一种新型的固相连接技术, 能够实现同种或异种金属之间的连接[1]. 与传统熔焊相比, 具有焊接变形小、残余应力小、无焊接热裂纹等优点[2-3].

搅拌摩擦焊实质是利用高速旋转的搅拌头与被焊工件之间的摩擦热, 同时被焊工件也受到搅拌头的挤压, 使其产生塑性金属而实现金属之间的连接, 因此, 摩擦热和塑性金属流动严重影响着焊接接头的力学性能, 国内外学者着重研究焊接接头温度场以及金属塑性流动特征[4-5]. 在焊接过程中, 焊缝金属经历了高温下的塑性变形, 而面心立方金属的塑性变形是通过位错的运动及相互作用来实现, 当晶粒受到搅拌针及轴肩的作用时, 滑移面与滑移方向沿一定方向转动, 最终达到面心立方金属中的稳定取向, 导致 FSW 焊缝中出现织构, 当材料中存在织构时, 表现为各向异性[6]. Suhuddin 等人[7] 研究表明, 由于搅拌针所引入的剪切应力, 匙孔周围形成{1 1 2} < 1 1 0 > 剪切织构, 而在远离匙孔区域, 焊核区经历了静态热处理, {1 0 0} < 1 0 0 > 立方织构占主导地位; 且轴肩对焊核区上表面晶粒取向有着显著的影响[8].

焊接过程中搅拌头转速影响着焊接接头微观组织[9], 因此, 文中以 6082-T6 铝合金 FSW 为研究对象, 应用瞬间急停–迅速冷却技术[7], 冻结焊接过程中焊核区上表面出现的晶粒取向; 采用电子背散射衍射 (EBSD) 技术, 研究不同转速焊接过程中晶粒形貌、晶粒尺寸、织构组分、晶界取向差的演化, 为 6082-T6 铝合金的广泛应用提供理论依据.

1 试验方法

试验材料选用厚度为 2 mm 的 6082-T6 铝合金, 焊接试板尺寸为 100 mm × 50 mm × 2 mm, 成分如表 1 所示.

使用柱状搅拌头将铝合金试板沿轧制方向进行对接, 轴肩直径 10 mm, 搅拌针直径 2 mm, 针长 1.8 mm, 焊接速度 80 mm/min, 转速分别为 1 200, 2 000 r/min, 搅拌头倾角 3°, 下压量 0.1 mm. 当搅拌头行走 80 mm 时, 立即按下急停按钮, 启动急停系统, 同时用冰水混合物冻结其动态组织. 母材及焊核区用线切割截取 EBSD 试样, 取样位置如图 1 所示, 区域 1 位于焊缝正中心, 距离匙孔 40 mm, 即焊接达到准稳态后的组织, 当 FSW 达到准稳态

收稿日期: 2018 − 11 − 30

基金项目: 国家自然科学基金资助项目 (2012ZX04008011)

表 1　6082 铝合金的化学成分 (质量分数，%)

Table 1　Nominal compositions of the 6082 aluminum alloy employed in this work

Si	Mg	Cu	Ti	Fe	Cr	Zn	Al
0.97	0.67	0.07	0.01	0.37	0.01	0.06	余量

后峰值温度出现在焊核区上表面，大约为 480 ℃[10]. 为了观察焊接过程中焊核区动态组织，采用“Stop-action”技术将被焊工件冷却，以减少因焊后热循环而产生的静态再结晶及晶粒长大. 母材及区域 1 试样上表面经砂纸粗磨、机械抛光后，在 10% 高氯酸无水乙醇溶液中进行电解抛光，抛光电压为 20 V，抛光液温度−20 ℃，抛光时间 40 s. 采用带有 EBSD 探头 (AztecX-Max80) 和 Channel 5 取向分析系统的场发射扫描电子显微镜 (Quanta 450 FEG) 进行电子背散射衍射试验，测试电压为 20 kV. 分析过程中，参考坐标系如图 1 所示，焊接方向 (WD)，横向 (TD) 和法向 (ND)，织构以 (h k l)[u v w] 形式表达，其中 (h k l) 为垂直于 ND 方向晶体的晶面，而 [u v w] 为平行于 TD 方向的晶向. 定义取向差为 2°～15°的晶界为小角度晶界，大于 15°则为大角度晶界，图 2c 中用灰色线表示小角度晶界，黑色线表示大角度晶界；按等效直径法计算平均晶粒尺寸.

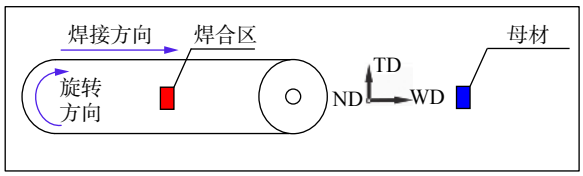

图 1　焊接方向和轴肩旋转方向以及 EBSD 试样取样位置示意图

Fig. 1　Schematic diagram of welding direction and rotation direction and the rectangles in black showing the locations of the EBSD maps

2　试验结果及分析

2.1　晶粒形貌分析

图 2a～2c 分别为母材、搅拌头转速为 1 200，2 000 r/min 时焊合区的晶粒形貌及晶界分型图，按等效直径法计算平均晶粒尺寸，母材平均晶粒为 25 μm，其晶粒间取向差接近于自由取向差 (图 3)，晶粒没有明显的择优取向；图 2b 显示转速为 1 200 r/min 时焊核区晶粒形貌，可以看出细小等轴晶均匀的分布于焊核区，平均晶粒大小为 3 μm，这是由于在焊接过程中，由轴肩及搅拌针所引入的剪切应力首先使母材粗大晶粒发生塑性变形，然后经历动态回复再结晶所致[11]；图 1c 显示转速为 2 000 r/min 焊核中心晶体形貌，与前者相比，随着搅拌头转速的提高，焊接过程中产热更多，达到了更高的瞬时温度，同时也经历了更高的焊后热循环温度，使焊合区细小晶粒进一步长大，其平均晶粒大小为 6 μm.

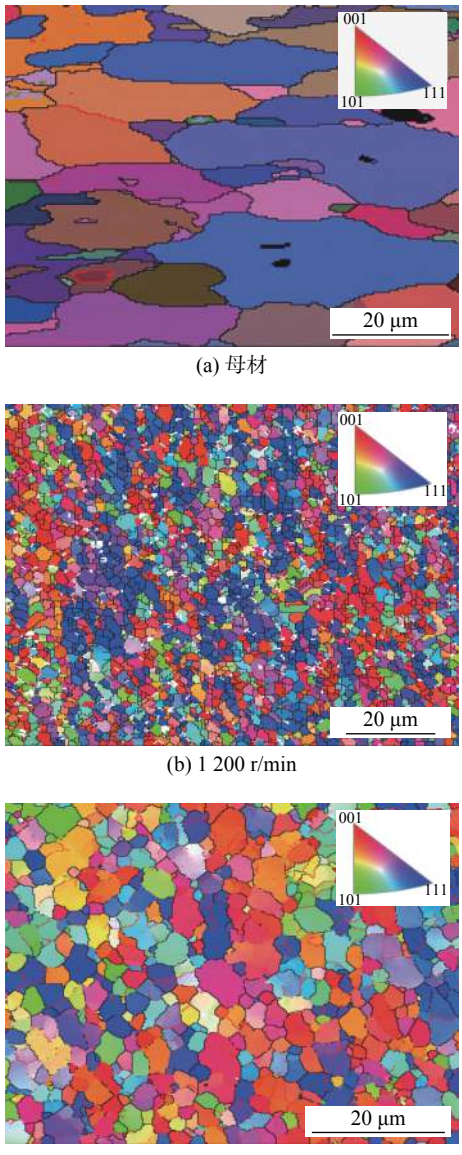

(a) 母材

(b) 1 200 r/min

(c) 2 000 r/min

图 2　EBSD 晶粒形貌及晶界分型图

Fig. 2　EBSD images of grains and boundaries type

2.2　晶界特征分析

图 3 给出了测试区的晶粒间取向差分布，由

图 3 可知, 从母材到焊合区, 小角度晶界组分明显增多, 而大角度晶界组分减少, 这是由于在 FSW 焊接过程中, 母材受到搅拌针及轴肩的挤压, 使焊合区具有软取向因子的晶粒发生塑性变形, 晶粒内的位错密度升高, 导致小角度晶界组分增加. 但在随后的动态回复再结晶过程中, 通过形核新的晶粒, 部分小角度晶界转变成大角度晶界, 从小角度晶界向大角度晶界的转变, 也是焊接过程中晶粒细化机理. 随着搅拌头转速的提高, 小角度晶界组分明显减少, 这是由于当搅拌头转速提高时, 焊接过程中达到了更高的瞬时温度, 也经历了更高的焊后热循环温度, 焊合区晶粒间的应力得到了释放, 使更多的小角度晶界转化为大角度晶界.

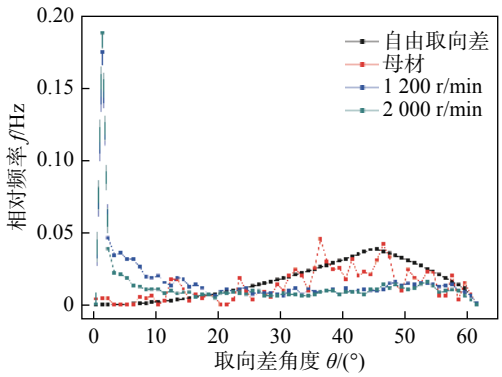

图 3 晶粒间的取向差分布

Fig. 3 Misorientation angle distribution histogram plots

2.3 织构分析

采用牛津公司开发的 Channel 5 软件进行织构分析, 表 2 是通过此软件计算得出的对应不同转速下焊核区中织构类型及其体积分数, 图 4 中的颜色与表 2 中的色型相对应, 不同的颜色代表不同的织构, 即不同的欧拉角或取向.

表 2 焊核区中常见面心立方金属织构及含量 (%)

Table 2 Fraction of Common textures in welding nugget

色码类型	转速1 200 r/min 取向(h k l)[u v w]	体积分数	色码类型	转速2 000 r/min 取向(h k l)[u v w]	体积分数
	(110)[001]	16.4		(100)[011]	21.8
	[110]//TD	24		[110]//TD	49.2
	(112)[11$\bar{1}$]	16.3		(11$\bar{1}$)[112]	16.4
	(114)[22$\bar{1}$]	19.4	—	—	—

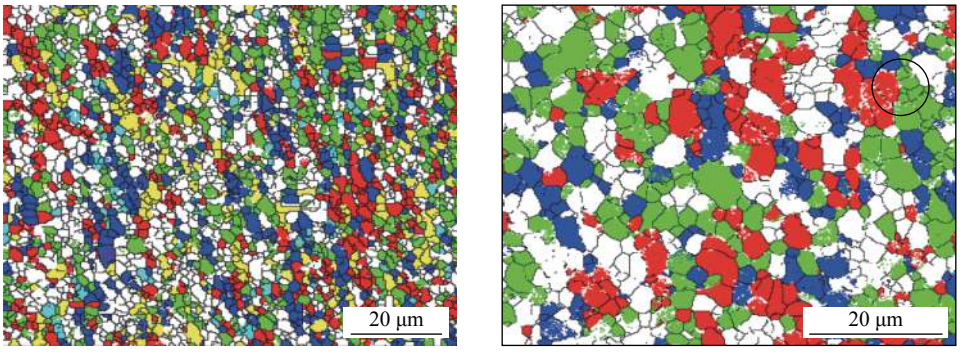

(a) 1 200 r/min (b) 2 000 r/min

图 4 不同织构对应的晶粒色差与分布

Fig. 4 Grains distribution of various textures

由图 4a 和表 2 可知, 当搅拌头转速为 1 200 r/min 时, 焊核区中的织构主要有 (110)[001] 高斯织构、(114)[22$\bar{1}$] 织构、(112)[11$\bar{1}$] 铜织构及 (110) 丝织构. 而 (110)[001] 高斯织构与 (114)[22$\bar{1}$] 织构之间有着特定的晶体学关系, (110)[001] 高斯织构与 (114)[22$\bar{1}$] 织构共享 (111) 晶面及 [110] 晶向, 而此 [110] 晶向位于 (111) 晶面上, 因此这两种织构关于 (111) 面对称[12]. 晶粒所处的应力状态决定着晶粒最终的取向, 对面心立方结构的金属来说, 最大剪切应力方向为 (111) 面上的 [110] 方向, 而在搅拌摩擦焊接过程中, 所形成的汤姆森四面体中 (111) 面大致平行于搅拌针的切面, 而 [110] 方向平行于搅

拌针的切线[13-14]. 因此在焊接过程中, 由于搅拌针的旋转所引入的剪切应力, 基于 (110)[001] 高斯织构与 (114)[22$\bar{1}$] 织构之间特定的晶体学关系, 首先, 同时形成 (110)[001] 高斯织构与 (114)[22$\bar{1}$] 织构; 其次, 以 (110)[001] 高斯织构与 (114)[22$\bar{1}$] 织构为基础, 在轴肩的顶锻压力作用下, 启动其 a1: (111)[01$\bar{1}$], a2: ($\bar{1}\bar{1}\bar{1}$)[$\bar{1}$01], b1: ($\bar{1}$11)[110], b2: (1$\bar{1}$1)[110] 主滑移系, 晶粒内发生塑性变形, b1, b2 滑移系致使此晶粒围绕 TD 方向旋转, 当旋转角度为 15°时, (114)[22$\bar{1}$] 取向晶粒其演变为 (112)[11$\bar{1}$] 取向, 演变过程示意图如图 5 所示. 随着搅拌头转速的提高, 焊核区经历了更多的塑性变形, 使 (112)[11$\bar{1}$] 取向晶粒继续沿 TD 方向旋转, 当旋转角度为 5°时, 进一步形成 (100)[011] 剪切织构; 当旋转角度为 20°时, 产生 (11$\bar{1}$)[112] 织构, 因此搅拌头转速为 2 000 r/min 时, (110)[001] 高斯织构、(114)[22$\bar{1}$] 织构全部演变为 (100)[011] 剪切织构和 (11$\bar{1}$)[112] 织构.

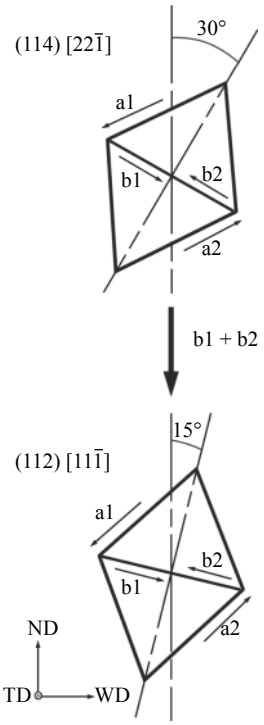

图 5　不同取向晶粒中激活的八面体滑移系示意图
Fig. 5　Schematic illustrations depicting slip systems

当面心立方金属受到挤压时, 产生 [110] 丝织构[15], FSW 焊接过程中焊核区主要受到搅拌针的旋转所引入的剪切应力, 而此应力平行于搅拌针的切线, 因此使焊核区部分晶粒的 [110] 晶向平行于 TD, 形成 [110] 丝织构. 随着搅拌头转速的提高, 晶粒内的塑性变形程度越严重, [110] 丝织构的组分显著增加. 具有相同取向的晶粒有一定的团簇现象, 如图 4b 中黑色圈指示, 特定的簇团内, 晶粒有相同的取向; 而不同的簇团均匀地分布于焊核区. 这是由于在焊接过程中, 应力不均匀所致, 当应力水平不高时, 晶粒内的塑性方式以滑移为主, 形成 (001)[110] 等板织构, 随着应力水平的提高而形成 [110] 丝织构, 而 [110] 丝织构的形成, 部分应力得到了释放, 邻近区域再次形成板织构. 在整个连续的焊接过程中, 高应力区域与低应力区域交替出现, 最终导致 (112)[11$\bar{1}$] 等板织构与 [110] 丝织构交替出现.

3　结　　论

(1) 搅拌摩擦焊焊接过程中, 由轴肩及搅拌针所引入的剪切应力, 使母材粗大晶粒发生塑性变形及动态回复再结晶, 母材粗大晶粒被细化, 随着搅拌头转速的提高, 焊核区经历了更高的热循环温度, 细小晶粒进一步长大.

(2) 基于搅拌针后方所形成的汤姆森四面体及 (110)[001] 高斯织构与 (114)[22$\bar{1}$] 织构之间特定的晶体学关系, 焊核区首先形成 (110)[001] 高斯织构和 (114)[22$\bar{1}$] 织构, 当搅拌头转速提高到 2 000 r/min 时, [110] 丝织构组分显著增加.

(3) 轴肩的顶锻压力使焊核区晶粒内发生塑性变形, 晶粒沿 TD 方向旋转, 随着搅拌头转速从 1 200 r/min 提高到 2 000 r/min 时, 焊核区经历了更多的塑性变形, 晶粒沿 TD 方向旋转角度增加, 进一步形成 (100)[011] 剪切织构和 (11$\bar{1}$)[112] 织构.

参考文献:

[1] Threadgill P L. Terminology in friction stir welding[J]. Science & Technology of Welding & Joining, 2007, 12(4): 357 − 360.

[2] Su J Q, Nelson T W, Mishra R, *et al*. Microstructural investigation of friction stir welded 7050-T651 aluminium[J]. Acta Materialia, 2003, 51(3): 713 − 729.

[3] Topic I, Höppel H W, Göken M. Friction stir welding of accumulative roll-bonded commercial-purity aluminium AA1050 and aluminium alloy AA6016[J]. Materials Science & Engineering A, 2009, 503(1): 163 − 166.

[4] 董学伟, 黎向锋, 左敦稳, 等. 7022 铝合金搅拌摩擦焊接全过程温度场的数值模拟 [J]. 机械工程材料, 2012, 36(10): 92 − 96.
Dong Xuewei, Li Xiangfeng, Zou Dunwen, *et al*. Numerical simu-

lation welding of temperature field in the process for 7022 aluminum full friction stir alloy[J]. Materials for Mechanical Engineering, 2012, 36(10): 92 − 96.

[5] 王希靖, 韩晓辉, 李常锋, 等. 厚铝合金板搅拌摩擦焊塑性金属不同深度的水平流动状况 [J]. 中国有色金属学报, 2005, 15(2): 198 − 204.
Wang Xijing, Han Xiaohui, Li Changfeng, *et al*. Horizontal flow status ofplasticmetal in differentdepth during friction stir welding for thick alum inum alloy[J]. Transactions of Nonferrous Metals Society of China, 2005, 15(2): 198 − 204.

[6] Xu W F, Liu J H, Chen D L. Material flow and core/multi-shell structures in a friction stir welded aluminum alloy with embedded copper markers[J]. Journal of Alloys & Compounds, 2011, 509(33): 8449 − 8454.

[7] Suhuddin U F H R, Mironov S, Sato Y S, *et al*. Grain structure and texture evolution during friction stir welding of thin 6016 aluminum alloy sheets[J]. Materials Science & Engineering A, 2010, 527(7-8): 1962 − 1969.

[8] 袁鸽成, 梁春朗, 刘 洪, 等. 搅拌摩擦焊焊接 5083 铝合金板材焊核区的晶体取向 [J]. 焊接学报, 2014, 35(8): 79 − 82.
Yuan Gecheng, Liang Chunlang, Liu Hong, *et al*. Crystal orientation in nugget zone of friction stir welded 5083 aluminum alloy plates[J]. Tansactions of the China Welding Instiution, 2014, 35(8): 79 − 82.

[9] 张洪武, 张 昭, 陈金涛. 搅拌摩擦焊接过程中搅拌头转速对材料流动的影响 [J]. 金属学报, 2005, 41(8): 853 − 859.
Zhang Hongwu, Zhang Zhao, Chen Jintao. Effect of angular velocity of the pin on materal folw during friction stir welding[J]. Acta Metallurgica Sinica, 2005, 41(8): 853 − 859.

[10] 王希靖, 韩晓辉, 郭瑞杰, 等. 搅拌摩擦焊接过程温度场数值模拟 [J]. 焊接学报, 2005, 26(12): 17 − 20.
Wang Xijing, Han Xiaohui, Guo Ruijie, *et al*. Numberical simulation of temperature field in friction stir welding[J]. Tansactions of the China Welding Instiution, 2005, 26(12): 17 − 20.

[11] 张成聪, 常保华, 陶 军, 等. 2024 铝合金搅拌摩擦焊过程组织演化分析 [J]. 焊接学报, 2013, 34(3): 57 − 60.
Zhang Chengcong, Chang Baohua, Tao Jun, *et al*. Microstructure evolution during friction stir welding of 2024 aluminum alloy[J]. Tansactions of the China Welding Instiution, 2013, 34(3): 57 − 60.

[12] Sato Y S, Kokawa H, Ikeda K, *et al*. Microtexture in the friction-stir weld of an aluminum alloy[J]. Metallurgical and Materials Transactions A, 2001, 32(4): 941 − 948.

[13] 胡庚祥, 蔡 珣, 戎咏华. 材料科学基础 [M], 上海: 上海交通大学出版社, 2000.

[14] Jeon J, Mironov S, Sato Y S, *et al*. Anisotropy of structural response of single crystal austenitic stainless steel to friction stir welding[J]. Acta Materialia, 2013, 61(9): 3465 − 3472.

[15] 张信钰. 金属和合金的织构 [M], 北京: 科学出版社, 1976.

第一作者简介: 张亮亮, 男, 1988 年出生, 博士研究生. 主要从事搅拌摩擦焊过程中组织演变方面的研究. Email: zll_0715@126.com

通信作者简介: 王希靖, 男, 教授, 博士研究生导师. Email: wangxj@lut.cn

In contrast, PF, whose dislocation density is small, is relatively pure and uniform. The heterogeneity of microstructures lead to a great dispersion of the fracture toughness of the weld metal, which is mainly due to the different fracture toughness and heterogeneous distribution of microstructures in crack tip.

Key words: weld metal; acicular ferrite; proeutectoid ferrite; fracture toughness

Prediction technology of electron beam welding deformation for aeroengine rotor components WANG Lun[1], PAN Bo[2], HUANG Yichen[2], LI Liqun[2] (1. Aero Engine Corporation of China, Shanghai 200241, China; 2. State Key Laboratory of Advanced Welding and Joining, Harbin Institute of Technology, Harbin 150001, China). pp 111-117

Abstract: The aircraft engine components require high dimensional accuracy, and the position of the core after welding cannot be machined. Therefore, the numerical simulation is used to predict the welding deformation of the rotor assembly. The experiment calculates the inherent strain value based on the theory of thermal elastoplasticity; calculate the inherent strain value of the electron beam welding of GH4169 alloy and analyze the influence of welding parameters on the inherent strain of the welding process; establish the structural model and analyze welding deformation of components under different welding parameters, sequences and fixtures. The result shows that the fourth-stage disc core has the largest axial deformation compared to the first, second and third discs, and the welding deformation can be effectively reduced by increasing the scanning speed and changing the fixtures. Therefore, the welding deformation of rotor assembly can be successfully predicted.

Key words: thermal elastoplastic theory; inherent strain method; welding deformation prediction

Prediction of welding distortion of large scale welded platform structure ZHANG Jiwei[1], LI Hongjia[2], FENG Zhongzhi[1], FANG Hongyuan[2] (1. 63926 troops of Chinese People's Liberation Army, China; 2. State Key Laboratory of Advanced Welding and Joining, Harbin Institute of Technology Harbin 150001, China). pp 118-122

Abstract: In order to carry out welding distortion prediction of large scale thick plate welded platform structure, a mock-up was welded first using actual welding process, during which angular distortion induced by welding was measured. And then welding numerical simulations of mock-ups having actual number of bead and lumped number of bead were conducted to verify the accuracy of the relevant input parameters of welding FE model and the reasonableness of the lumped-weld scheme by comparing their angular distortion results. Finally, welding FE model of the platform was established based on the scheme of lumped-weld, and welding induced distortion of the structure was analyzed. The results shows that the angular distortions of FE model and lumped-weld FE model are both similar to the test value of the mock-up, which is about 1.6°. That is to say the accuracy of the lumped-weld scheme that simplifies the 15-layer 27-pass in actual welding process to 5-layer 5-pass was verified. The welding distortion of the platform structure is localized falling or convex outward deformation resulting from welding angular distortion caused by the asymmetry of the upper and lower grooves and the support effect of the bottom steel frame. The surface outward deformation range is about −5.2 to 4.4 mm.

Key words: platform structure; welding distortion prediction; lumped-weld; numerical simulation

Effect of misalignment on fatigue performance of horizontal welded joints in steel catenary riser system WANG Zhen[1], CHENG Fangjie[1,2], ZHANG Yanshen[1], SHAO Zhujing[1], WANG Dongpo[1,2] (1. School of Materials Science and Engineering, Tianjin University, Tianjin 300072, China; 2. Tianjin Key Laboratory of Advanced Joining Technology, Tianjin 300072, China). pp 123-127

Abstract: In order to investigate the effect of misalignment on the horizontal girth weld fatigue performance, the joints of steel catenary riser were welded by TIG welding with filler wire and the fatigue tests of the joints were carried out at the stress range of 80, 120 and 175 MPa, respectively. The results indicated that the misalignment mode has a significant influence on the fatigue cracking initiation position of horizontal welding joints. The fatigue crack of upper-misalignment-joint is almost from the upper side of the root toe, and the fatigue crack of joints without misalignment is mainly from the bottom of the root toe, besides, the fatigue crack of down-misalignment-joint is all from the bottom of the root toe. In addition, the fatigue endurance of the specimens is decreased continuously with the increase of the misalignment values at the same stress range, and which is reduced obviously when the misalignment values exceed 0.60 mm.

Key words: steel catenary riser; horizontal welding; misalignment; fatigue performance; cracking location

Effect of rotation speed on texture type in friction stir welding joint for 6082-T6 aluminum alloy ZHANG Liangliang[1], WANG Xijing[1,2], WEI Xueling[1], LIU Xiao[1], CHAI Tingxi[3] (1. State Key Laboratory of Advanced Processing and Recycling of Non-ferrous Metals, Lanzhou University of Technology, Lanzhou 730050, China; 2. School of Materials Science and Engineering, Lanzhou University of Technology, Lanzhou 730050, China; 3. School of Bailie Mechanical Engineering, Lanzhou City University, Lanzhou 730070, China). pp 128-132

Abstract: The evolutions of grain morphology, grain boundary features and texture components on the upper surface of friction stir welding nugget for 6082-T6 aluminum alloy at different rotation speeds of tool were studied by electron backscatter diffraction technology combined with orientation analysis software. The results indicated that the (110) [001] Goss texture and (114)[22$\bar{1}$] texture were formed in the nugget zone under the shear stress introduced by the pin, and the upsetting pressure of the shoulder made it rotate to certain angle along the transverse direction, leading to the formation of (112)[11$\bar{1}$] copper texture. With elevating the rotation speed of tool, the rotation angle of grains along the transverse direction increased, resulting in the further formation of (100) [011] shear texture and (11$\bar{1}$)[112] texture. [110] fiber texture was formed by extrusion of grain in nugget zone by pin. When the rotation speed of tool was elevated from 1 200 to 2 000 r/min, the extrusion degree was increased, which resulted in a

significant increase in the components of [110] fiber texture.

Key words: 6082-T6 aluminum alloy; friction stir welding; grain orientation evolution; EBSD

Study on the microstructure and properties of the laser welding of GTi70 and TC4 dissimilar materials WANG Weixin[1,2], FU Xingbai[1], LIU Jufeng[1,2], WANG Huaqiao[1] (1. Hubei Hongyang Sanjiang Aerospace Electromechanical Co.,Ltd., Xiaogan 432100, China; 2. Hubei Province Key Laboratory of Advanced Welding Technology, 432100, China). pp 133-139

Abstract: This paper concentrates on the welding performance of GTi70 and TC4 dissimilar materials. The microstructure and mechanical properties of the welded joint with laser welding were investigated, which shows the weld ability of GTi70 and TC4. The micro structures and fracture morphologies of the welded joint were analyzed through OM, XRD and SEM, and the detailed analysis of tensile strength were performed. The results demonstrated that the tensile strength of welding joints were higher than GTi70 at room temperature, while the tensile strength was higher than TC4 at 500, 600 and 750 °C. The tensile fracture and shear fracture of welded joint were plastic fractures. In addition, compared to continuous laser welding seam, the micro structure and mechanical properties of pulsed laser welding seam were better.

Key words: high temperature titanium alloy; dissimilar material welding; pulsed laser welding; weld microstructure

Study on microstructure and microhardness of linear friction welded joints of Ti-22Al-27Nb alloy CHANG Chuanchuan, ZHANG Tiancang, LI Ju (Aeronautical Key Laboratory for Welding and Joining Technologies, AVIC Manufacturing Technology Institute, Beijing 100024, China). pp 140-144

Abstract: In this paper, the Ti-22Al-27Nb based alloy was welded by linear friction welding (LFW), and then subjected to post-weld heat treatment. The microstructure and the microhardness of the linear friction welded joints were investigated. The results showed that the sound joints free of defects can be obtained by using LFW method. As welded condition, the weld zone is mainly composed of metastable B2 phase. In thermo-mechanically affected zone, equiaxial α_2 occurred in this zone and the acicular O phase nearly disappeared. After heat treatment, the lath O phase and acicular O phase precipitated at weld zone, the thermo-mechanically affected zone is a two-phase region with uniform distribution of O phase. The microhardness of base material is about 300 HV, the microhardness increases with approaching to weld center, which maximum microhardness is 354 HV. After heat treatment, the microhardness of the weld center increased sharply due to precipitation of lath O and acicular O phase.

Key words: Ti-22Al-27Nb; linear friction welding; microstructure; microhardness

Influence of micro-arc oxidation film on corrosion of inhomogeneity of 7A52 aluminum alloy friction stir welding joint HAO Lixin[1,2], JIA Ruiling[1], ZHANG Huixia[2], ZHAI Xiwei[1], CHEN Furong[1] (1. Key Laboratory for Thin Film and Coatings of Inner Mongolia Autonomous Region, Inner Mongolia University of Technology, Hohhot 010051, China; 2. State Key Laboratory for Marine Corrosion and Protection, Luoyang Ship Material Research Institute(LSMRI), Qingdao 266101, China). pp 145-150

Abstract: Due to dynamic recrystallization of the 7A52 aluminum alloy friction stir welding joint weld zone. The grain size is relatively small, the organization presents "onion ring" distribution. the thermo mechanically affected zone is distributed along the plastic flow direction, and the grain size of the heat affected zone is obviously grown. The unevenness of the joint structure leads to different corrosion behaviors in different regions. The results show that when there is no micro-arc oxide film, the blunt current of the base material is much smaller than that of the weld nugget area and the heat(thermo mechanically) influence zone, and it is easier to passivate; when the thickness of the micro-arc oxide film is 50 μm, the base material is blunt The current is less than the weld nugget zone and the heat(thermo mechanically) influence zone. The thinner micro-arc oxide film has no obvious effect on the improvement of joint corrosion inhomogeneity; when the thickness of the micro-arc oxide film is 70 μm, the passivation characteristics of different regions of the joint are closing, the micro-arc oxide film helps to reduce the influence on the unevenness corrosion of joint structure in different areas of the joint.

Key words: 7A52 aluminum alloy; friction stir welding; corrosion; micro-arc oxidation

Analysis of microstructure and mechanical properties of resistance spot welded 22MnB5 hot stamping steel CAI Helong, YI Hongliang, WU Di (The State Key Laboratory of Rolling and Automation, Northeastern University, Shenyang 110819, China). pp 151-154

Abstract: 22MnB5 hot stamping steel was resistance spot welded using different welding procedures. The effects of welding parameters on weldability were investigated, and the microstructural evolution of spot weld and the relation of microstructure-mechanical performance were studied. The results show that there is a positive correlation between nugget diameter and tensile shear load. Compared to electrode force, welding current displays a more critical effect on mechanical performance of spot weld. The difference in micro-hardness across the whole weld is determined by the microstructural evolution. Fully martensitic microstructure appears in the whole weld, except for inter-critical heat affected zone(IC-HAZ), which has the lowest hardness due to a duplex microstructure of ferrite and martensite. This softening phenomenon improves load-carrying capacity and energy absorption of spot weld in mechanical failure condition, leading to the occurrence of pullout failure mode.

Key words: resistance spot welding; hot stamping steel; mechanical properties; softening zone

Reviews on welding method of SiC particle reinforced aluminum matrix composites NIU Jitai[1,2,3], CHENG Dongfeng[1,2], Gao Zeng[1,2], WANG Peng[1] (1. College of Materials Science and Engineering, Henan Polytechnic University, Jiaozuo 454003, China; 2. Engineering Research